INTERNATIONAL JOURNAL FOR NUMERICAL METHODS IN FLUIDS, VOL. 18, 871–886 (1994)

THE EFFECTS OF FLOW SPLIT RATIO AND FLOW RATE IN MANIFOLDS

H. FU

Centre for Heat Transfer and Fluid Flow Measurement, School of Physical Sciences and Engineering, King's College London, Strand, London WC2R 2LS, U.K.

A. P. WATKINS*

Department of Mechanical Engineering, UMIST, PO Box 88, Manchester M60 1QD, U.K.

AND

M. YIANNESKIS

Centre for Heat Transfer and Fluid Flow Measurement, School of Physical Sciences and Engineering, King's College London, Strand, London WC2R 2LS, U.K.

SUMMARY

This paper reports a combined experimental and numerical investigation of three-dimensional steady turbulent flows in inlet manifolds of square cross-section. Predictions and measurements of the flows were carried out using computational fluid dynamics and laser Doppler anemometry techniques respectively. The flow structure was characterized in detail and the effects of flow split ratio and inlet flow rate were studied. These were found to cause significant variations in the size and shape of recirculation regions in the branches, and in the turbulence levels. It was then found that there is a significant difference between the flow rates through different branches.

The performance of the code was assessed through a comparison between predictions and measurements. The comparison demonstrates that all important features of the flow are well represented by the predictions.

KEY WORDS Manifolds Pipe junctions Laser anemometry Computational fluid dynamics Intake manifolds Inlet manifolds

1. INTRODUCTION

The behaviour of the intake system plays a critical role in engine performance, because it governs the air flow into the internal combustion engine cylinders. The inlet manifold is one of the main components of the intake system and needs to be designed to give low air resistance and good distribution of air or mixture between cylinders and to take advantage of ram and tuning effects. The details of the air flow are extremely complex. In order to investigate the flows in manifolds, both experimental and numerical studies have been carried out. Margary and Nino[1] measured the instantaneous mass flow rate of the inlet flow and the in-cylinder swirl velocity and found that even in single-cylinder engines the intake duct length alone can have a complex effect on the volumetric efficiency and swirl velocity in the cylinder. Arcoumanis *et al.*[2] investigated the

* Author to whom correspondence should be addressed.

CCC 0271–2091/94/090871–16

Received August 1993
Revised December 1993

unsteady flow in the inlet manifold of a production diesel engine under motored conditions by laser Doppler anemometry and found that a very complex flow is present in the plenum of the manifold. Computer simulations of the unsteady fluid dynamics in engine manifolds, employing one-dimensional techniques such as the method of characteristics and also finite difference techniques, have been used extensively in both universities and industry.[3,4] However, being one-dimensional, these techniques are unable to fully predict the flow field, so they are not appropriate for the assessment of the effects of the geometry of manifold components, such as the shape of the cross-section of the ducts, the angle and location of the junctions between the plenum and the branches, etc. With the rapid increase in computer capacity and speed in recent years and the improved capabilities of computer methods, multidimensional simulations have been attempted. Pollard and Spalding[5] examined the dividing flow in a symmetric T-junction. Chapman[6] used a two-dimensional compressible hydrodynamic model to simulate the manifold flow. Leschziner and Dimitriadis[7] applied a steady three-dimensional code to the joining flow in a pulse converter junction of an exhaust system. Fu *et al.*[8] reported a three-dimensional numerical study of the steady non-symmetric turbulent dividing flow in a single inlet manifold junction. However, there is still a need for information about multibranch flows which are encountered in multicylinder engines.

This paper presents a simulation of the three-dimensional incompressible steady turbulent flows through a two-branch manifold using a CFD method with the k–ε model of turbulence. In order to assess the numerical predictions, measurements of mean and RMS velocity components were obtained using laser Doppler anemometry (LDA) in a purpose-built water rig.

The work presented in this paper forms part of the first stage of a combined computational and experimental programme. Engine manifold flows are of course unsteady and compressible, but such aspects have not been considered in this stage of the work. It is useful to identify first the steady flow characteristics that affect the flow patterns.

To this end the effects on the flow of important parameters have been assessed. The two parameters investigated here are the flow split ratios between the branches and the main duct and the rate of the flow entering the main duct.

Most current IC engines have at least four cylinders, resulting in manifolds with at least four branches. The effects on the flow through the manifold of additional branches have been assessed elsewhere.[9]

2. MATHEMATICAL DESCRIPTION

The computer programme used for the present flow analysis was based on that developed by Leschziner and Dimitriadis.[10] It is written in terms of general curvilinear co-ordinate systems, allowing the use of non-orthogonal grids. However, for the present analysis the geometry is adequately described by a Cartesian co-ordinate system as shown in the inset of Figure 1. The flow domain consists of a square main duct of dimensions 50·8 mm × 50·8 mm × 430 mm and two branches of dimensions 30 mm × 30 mm × 194·2 mm placed centrally in the bottom wall of the main duct as shown. There is thus a main duct/branch area ratio of 2·87. For the calculations the central y–z plane in the main duct and branches is assumed to be a symmetry plane. Thus the flow in only half of the main duct and branches is solved.

The flow Reynolds number, based on the bulk velocity at the inlet of the main duct and on the hydraulic diameter (D = 50·8 mm), was 60,000 and the working fluid was water. The flow could therefore be expected to be fully turbulent. A turbulence model is thus required. For the present analysis the standard high-Reynolds-number k–ε model of Launder and Spalding[11] has

been adopted, coupled with wall functions to account for the laminar sublayers near the walls. It is recognized that this turbulence model may not be fully adequate for the complex flow through the branches. However, alternative, more accurate models such as the second-moment closure differential stress models of Launder[12] are much more difficult to converge to a solution and are therefore more expensive to run. They are not yet commonly used for large-scale three-dimensional flow problems, particularly when, as here, a parametric analysis involving a large number of separate runs of the programme is to be carried out.

The equations governing the flow were discretized using the hybrid scheme and the derived finite volume equations were solved with the SIMPLER algorithm of Patankar.[13] The scalar variables are stored at the grid nodes and the velocity components are arranged at staggered locations relative to the grid nodes. The zonal approach was employed in the calculation, as described by Dimitriadis and Leschziner.[14] The computational domain is divided into a number of duct zones, i.e. one zone comprising the main duct and one zone for each of the branches. The flow in each duct is computed separately by a single-duct module, with the interactions between zones being accounted for iteratively through an overlap of pressure and velocity nodes on or near the interfaces between the main duct and the branches.

The distributions of all dependent variables except the pressure were prescribed at the inlet plane of the main duct. The velocity distribution at the inlet plane measured by laser Doppler anemometry was used as the inlet condition for the computations. At the exit plane of the main duct the mass flow rate was specified and the condition $(\partial/\partial z)(\partial p/\partial z) = 0$ was prescribed. The pressures at exits of the branches were set to be equal and taken as a datum (zero value) and $(\partial/\partial y)(\partial p/\partial y) = 0$ was also imposed. Computations were performed with numerical mesh sizes of $10 \times 18 \times 87$ in the main duct and $7 \times 12 \times 62$ in each branch. It has previously been established by Fu *et al*[8] that a solution with a finer mesh size for a case with a single branch and the same inflow conditions showed no significant differences from that obtained with the grid employed in the present work.

The predictions of mean velocity, turbulence energy, pressure difference and flow distribution between the branches were validated against measurements obtained in a steady flow water rig. The experimental system has been described in detail in Reference 15.

3. RESULTS AND DISCUSSION

The main features of the flow can be observed from Figure 1, which shows the velocity vectors and streamlines in the plane of symmetry. For the results shown in this figure the bulk velocity and flow rate at the main duct inlet were $1{\cdot}27\ \mathrm{m\,s^{-1}}$ and $3{\cdot}3 \times 10^{-3}\ \mathrm{m^3\,s^{-1}}$ respectively and the flow split ratio (total branch flow rate/main duct inlet flow rate) was 0·23, i.e. 23% of the inlet flow entered the two branches.

Figure 1 shows that the flow upstream of the first junction (from left to right) in the main duct is very uniform and the velocity profiles are essentially unaffected by the branch. The symmetry in the y-direction of the flow about the axis of the main duct is well preserved and cross-stream motion is negligible up to the junction region. However, the flow downstream of the junctions is affected by the branches. The velocity at the bottom wall of the main duct downstream of the junctions is noticeably higher than that at the top wall owing to the convection of higher-axial-momentum fluid from the centre of the flow in the main duct caused by the flow into the branches.

A secondary flow is generated in cross-stream planes in the main duct downstream of the branches owing to the flow through the latter. The effects of this are transported downstream

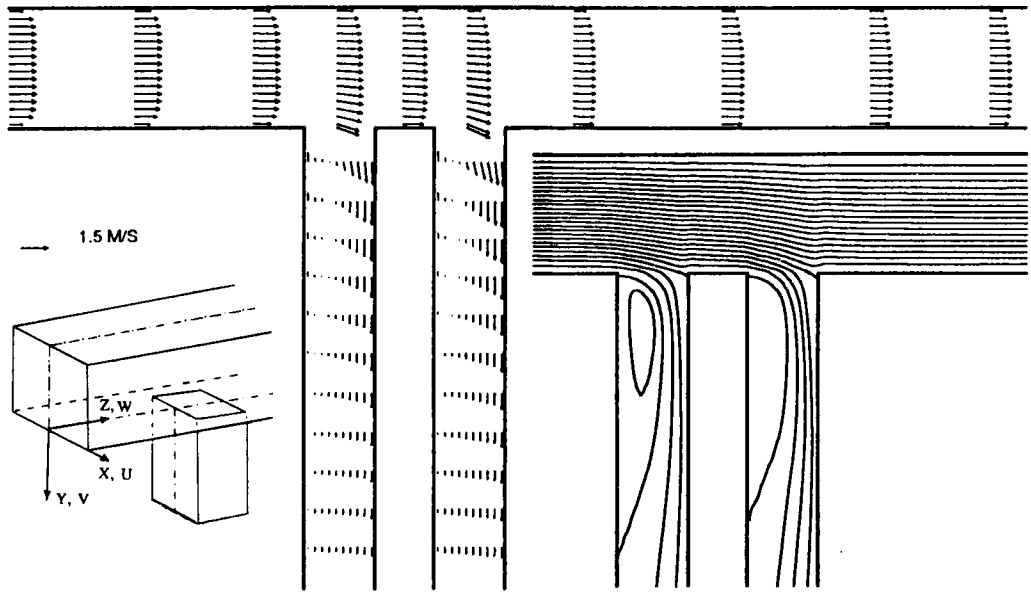

Figure 1. Velocity field and streamline pattern in plane of symmetry. Inlet flow rate $3{\cdot}3 \times 10^{-3}$ m^3 s^{-1} flow split ratio 23%

in the main duct, resulting in the impingement of the cross-stream flow on the bottom wall as shown in Figure 2. The secondary flow comprises two vortices, one on either side of the plane of symmetry of the flow, which by the $z = 7{\cdot}66D$ plane shown in Figure 2 occupy all of the duct cross-section. The magnitude of the secondary flow is small compared with that of the streamwise motion, being everywhere less than 2·5% of the bulk flow velocity in the main duct.

The flow separation in the branches is the main feature of the flow. The flow separates at the upstream corners of the junctions, undergoing significant streamline curvature in the process. A recirculation region is formed along the upstream wall of each branch. There is a difference in the sizes of the two recirculation regions. The reattachment point in the first branch is 15% further downstream than in the second branch. This was confirmed by laser Doppler anemometry measurements. Figure 3 presents the measured streamwise velocity profiles on the symmetry plane in the branches at distances of 36·4 and 104·0 mm from the main duct/branch interfaces. The reverse flow region for the first branch is wider than that in the second, indicating a wider recirculation region in the first branch. By the second station the velocities in the reverse flow region of branch 2 are very small, showing that this location is near the end of recirculation and that the recirculation region is shorter than that in branch 1.

The velocity distribution in the branches is highly non-uniform, with high velocities near the downstream walls. These velocities result from the acceleration of the flow outside the recirculation region, since it must flow over the widest part of the separated region. As a result there is a high velocity gradient and high shear stress on the downstream wall. This is illustrated in Figure 4, which shows the calculated shear stresses on the symmetry plane on the upstream and downstream walls of the two branches. The reverse velocities in the recirculation zone are relatively small and do not exceed 0·5 m s^{-1}. The velocity gradients near the branch exits indicate that the flow has not fully recovered and it can be expected to continue to recover further

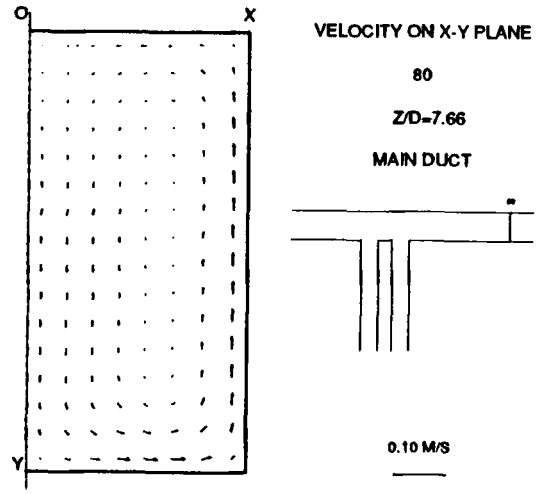

Figure 2. Cross-stream motions in main duct. Inlet flow rate $3{\cdot}3 \times 10^{-3}\ m^3\ s^{-1}$ flow split ratio 23%

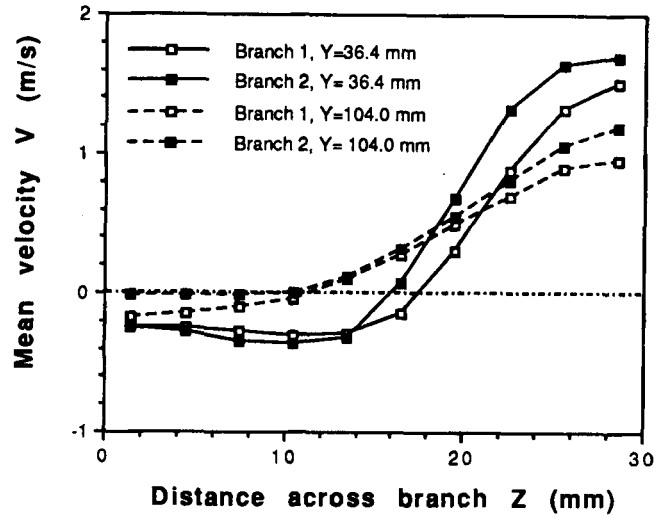

Figure 3. Measured streamwise velocity in branches. Inlet flow rate $3{\cdot}3 \times 10^{-3}\ m^3\ s^{-1}$ flow split ratio 23%

downstream. However, the exit plane is well downstream of the recirculation region and the prescribed exit boundary condition on pressure is clearly justified, as can be seen from Figure 5.

Figure 5 presents the pressure contours on the plane of symmetry. There are steep pressure gradients in the junction regions, with the highest pressures at the downstream corners of the interfaces where the fluid stagnates. The lowest-pressure regions are located near the upstream walls adjacent to the interfaces in the recirculating regions. The pressure distribution provides useful information for the interpretation of the velocity field. The large pressure gradient at the interface region changes the flow direction in the main duct and drives the flow into the branches. The recirculating flows may be also explained from the adverse pressure distribution in the branches.

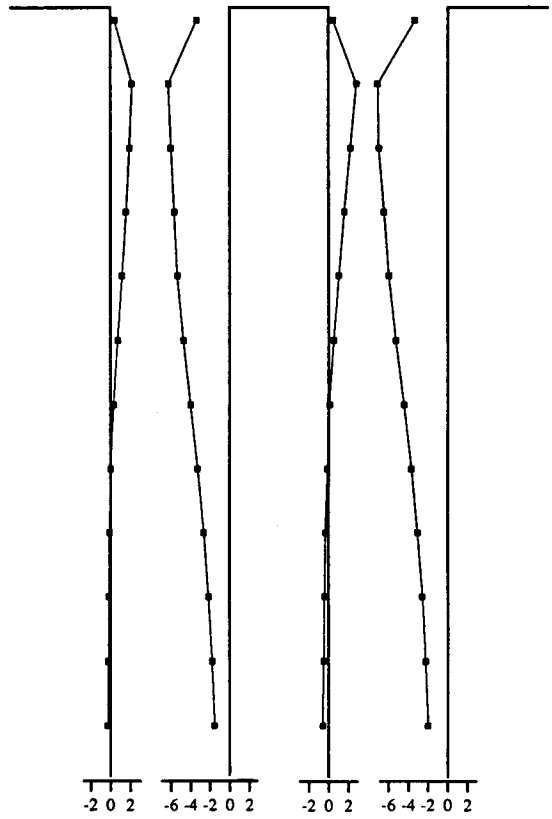

Figure 4. Calculated wall shear stresses in branches. Inlet flow rate $3{\cdot}3 \times 10^{-3}$ m^3 s^{-1} flow split ratio 23%

The pressure gradient varies in sign down the main duct. Before and after the junctions the pressure drops owing to friction. However, the pressure rises rapidly in the junction region because of the diminution of mass flow rate in the main duct. The overall effect for the cases examined here is such that the pressure at the exit of the main duct is higher than that at the entrance. Similarly, the pressure level at the entrance to the second branch is higher than that at the first junction, as illustrated in Figure 5. Another possible reason for this relates to the higher near-wall velocity in the main duct downstream of the first branch opening compared with that upstream (see Figure 1). In order to decelerate this velocity to zero at the downstream wall of the second branch, a stronger pressure gradient is required than at a similar position in the first branch. This results in higher pressures around the stagnation point in the second branch than in the first branch.

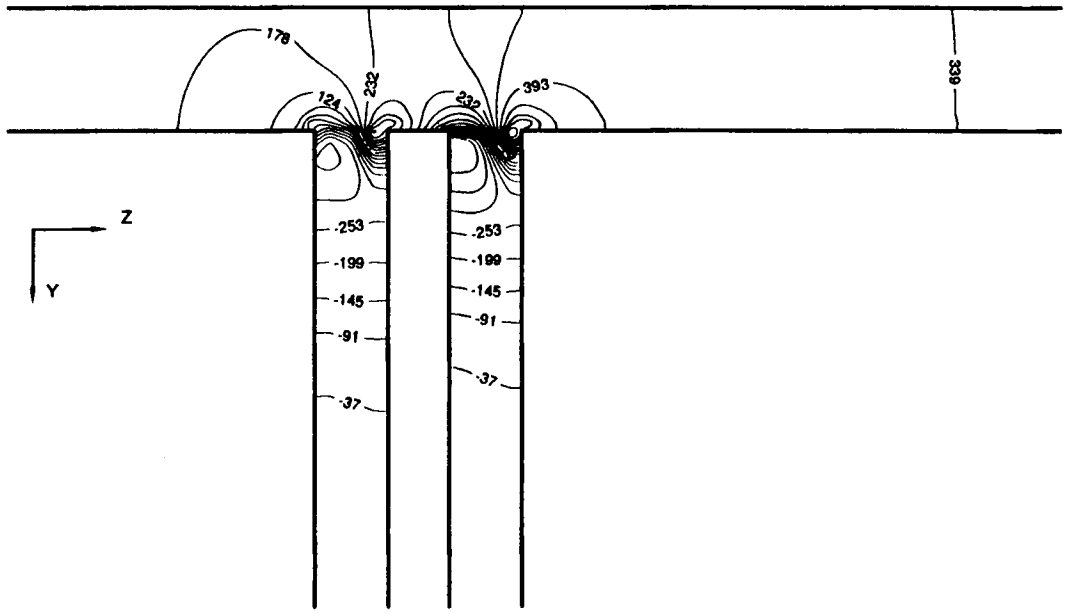

Figure 5. Pressure contours (values in pascals) in plane of symmetry relative to datum value at branch exits. Inlet flow rate $3{\cdot}3 \times 10^{-3}$ m^3 s^{-1} flow split ratio 23%

As a consequence of the higher pressures at the entrance to the second branch compared with the first and the fact that the same pressure level is maintained at the exits of the two branches, the flow rate through the second branch is 34% higher than that through the first branch. This is illustrated later in Figure 11 for the flow split ratio of 0·23. These findings were confirmed by flow rate and static pressure measurements in the rig, although (as also shown in Figure 11) the measured flow rate in the second branch is 70% higher than that in the first.

The larger flow rate through the second branch has a number of consequences. Figure 3 shows firstly that the forward flow in the second branch is everywhere of a higher velocity than that in the first branch. Secondly, as shown in Figure 5, the pressure is lower within the recirculation region in the second branch compared with the first. As a consequence, as illustrated in Figure 1, the separating streamline is forced further in towards the wall on which the recirculating region sits. Thus the recirculation region is narrower there or, in other words, the area made available for the forward flow is increased in the second branch.

Cross-stream motions are present throughout each of the branches. In the region close to the main duct/branch interface the secondary flows are complex vortical motions as shown in Figure 6(a). The vortical motion near the upstream wall (marked OX in Figure 6(a)) is very small, being everywhere less than 1% of the bulk velocity at the inlet to the main duct. The cross-stream motion in the lower part of Figure 6(a) corresponds mainly to the lateral movement of the primary flow, which is directed towards the downstream wall of the branch as it bypasses the recirculating fluid. Peak velocities are approximately 10% of the bulk flow at the inlet. Downstream of the reattachment point a single vortical motion persists and decays with distance from the interface, as shown in Figure 6(b); however, the velocities at the plane shown, $y = 6{\cdot}10d$, are very low and in general do not exceed 0·05 m s^{-1}. Similarly, a slightly stronger cross-stream motion exists in the second branch, as shown in Figure 6(c).

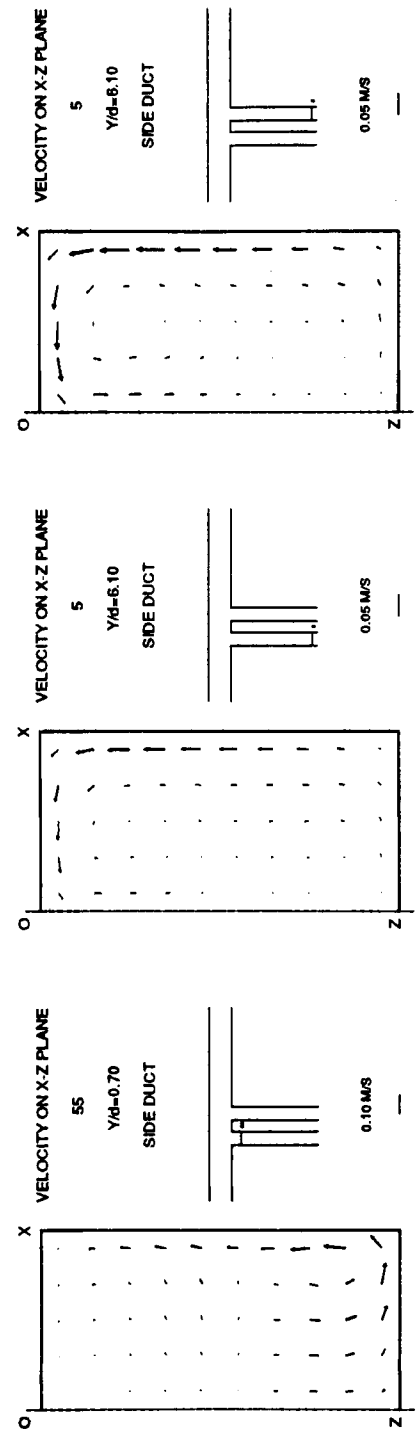

Figure 6. Cross-stream motions in branches. Inlet flow rate $3{\cdot}3 \times 10^{-3}$ m^3 s^{-1} flow split ratio 23%

Comparisons with experiment

In order to provide benchmark data appropriate for the development and assessment of the numerical code, detailed measurements of the mean velocity components and the corresponding turbulence levels, i.e. the RMS velocity components, were obtained by LDA.

The accuracy of the computed flow field can be assessed from the comparison. Figure 7 shows the measured and computed streamwise velocities on the symmetry plane for the two-branch flow discussed above. Within the main duct the agreement is excellent in the upstream, junction and downstream regions. It must be noted that in the upstream region of the main duct agreement is expected, since the experimental data were used as inlet conditions.

The agreement in the branches is less good. As can be seen in Figure 7, the peak velocity in the forward flow over the recirculation region is underpredicted by 20%. The shape of the profile is also incorrectly predicted, with the area covered by the backflow being substantially underpredicted, by 30%–40% in the profiles shown.

Figure 8 compares the measured and calculated RMS axial velocities. The latter are defined as $\sqrt{(\frac{2}{3}k)}$ assuming isotropic turbulence. The profile shapes are generally satisfactory, except in the recirculation regions in the branches. However, peak values in both the main duct and the branches are underpredicted by around 30% at maximum.

The discrepancies may be attributed to numerical diffusion and the shortcomings of the k–ε model in dealing with recirculating flows. It has generally been observed that the isotropic turbulent eddy viscosity relationship on which the k–ε model is based may lead to inaccuracies in recirculation flows.[16,17] Improvements in the prediction of recirculating flow may be achieved by better representation of turbulence. In many recirculating flows (see e.g. Reference 18) the dominant production of turbulence energy takes place through the interaction of the normal stresses with the normal strain rates. Effective viscosity models do not, however, represent

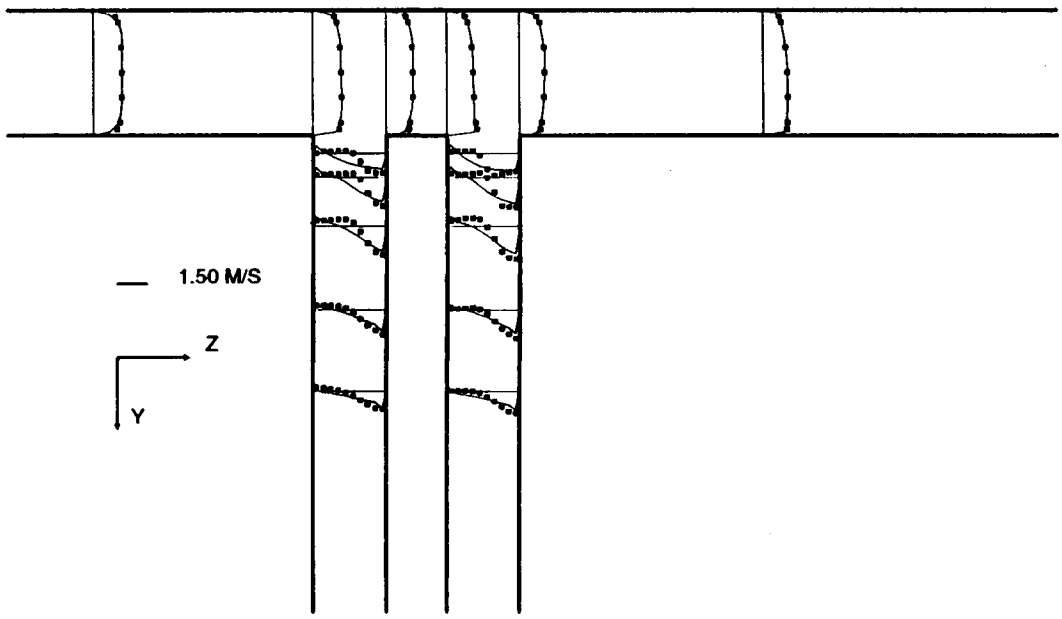

Figure 7. Comparison of predicted and measured axial velocity profiles. Inlet flow rate $3{\cdot}3 \times 10^{-3}$ m^3 s^{-1} flow split ratio 23%; ____, predicted; ■, measured

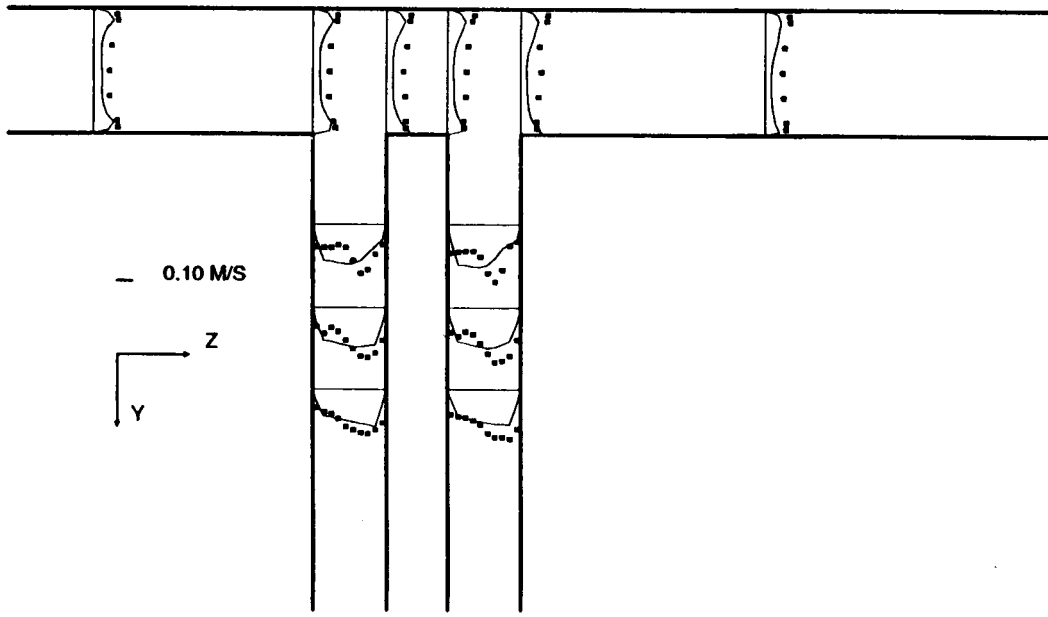

Figure 8. Measured and calculated axial RMS velocity profiles in plane of symmetry. Inlet flow rate $3{\cdot}3 \times 10^{-3}$ m^3 s^{-1} flow split ratio 23%; ____, predicted; ■, measured

sufficiently normal stresses. Numerical diffusion may be the cause of the predicted forward flow having a wider profile than it should, with consequent lower peak velocities. Recourse could be made to higher-order non-diffusive solution schemes, e.g. QUICK.[19] However, these are much more difficult to converge, resulting in greatly increased computing times.

Despite the discrepancies noted above, certain key features of the mean flow are correctly captured by the calculations. It has already been noted that the flow split between the branches is correctly predicted. The lengths of the recirculation regions in both branches are also predicted well. Although the widths of these regions are underpredicted, the predictions do give a wider region in the first branch compared with the second in agreement with the measurements. The computational model may therefore be expected to provide a reasonable description of the flow dynamics and produce correct predictions of the effects of variations in influential factors such as inlet conditions, flow split ratio, geometrical parameters, etc.

Effect of flow split ratio

In order to investigate the effect of the flow split ratio on the mean flow and turbulence structure, calculations were performed for three different flow split ratios, namely 23%, 46% and 68%, while the inlet flow rate in the main duct was held constant. The general pattern of the flow described above remained the same in all the cases examined.

However, the flows in the branches exhibit important differences in detail, as illustrated by the measurements shown in Figure 9. Because of the need for a greater flow rate through the branches at a higher flow split ratio, the forward velocities are greatly enhanced, with peak velocities increased by approximately 32% and 60% respectively at the two stations shown. At the same time the widths and lengths of the backflow regions are greatly reduced. As a consequence of the steeper mean flow gradients, the turbulence levels are generally increased by increasing the flow split ratio.

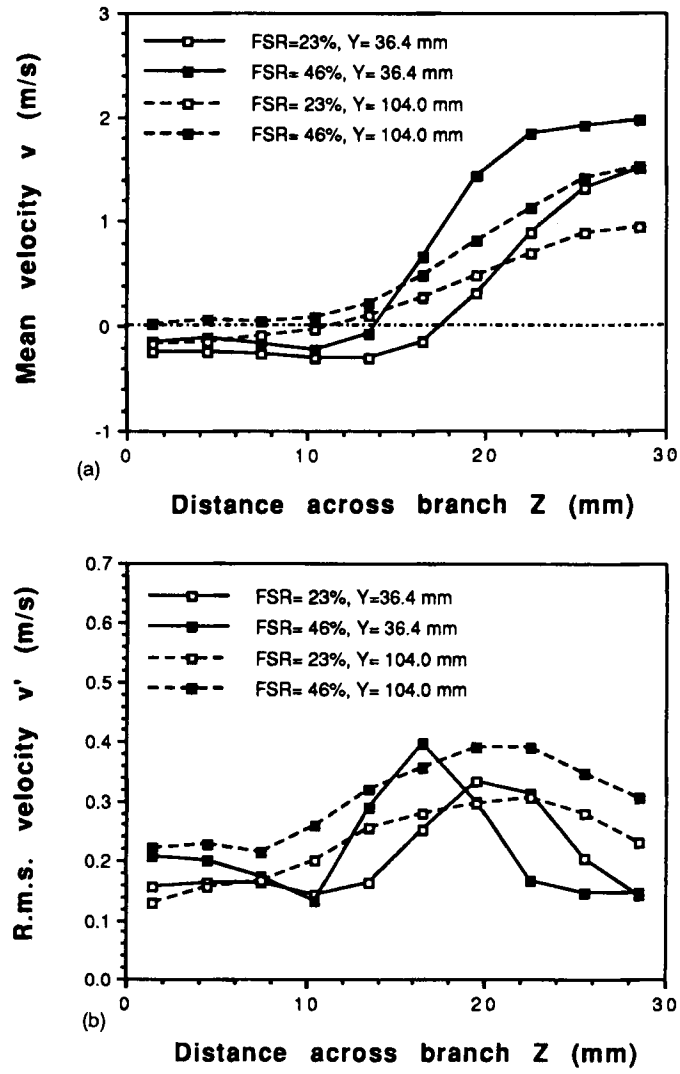

Figure 9. Effect of flow split ratio on axial (a) mean and (b) RMS velocity profiles in branch 1

Pressure levels are also raised by increasing the flow split ratio. Figure 10 shows the pressures at the inlet (P_1) and exit (P_2) of the main duct relative to the datum value at branch exits. These have been normalized by the pressure head plus velocity head ($p+\rho u^2/2$) at the main duct inlet. There is good agreement between the predictions and the measurements, with the former perhaps showing more variation, but generally there is a near linear variation in both P_1 and P_2 with flow split ratio. These increases in pressure levels can be explained by the need for higher pressure levels in the branch/main duct interface regions in order to drive more fluid through the branches. These higher pressure levels here then result in higher pressure levels at the main duct inlet in order to drive the flow towards the interface region. Finally, because the flow rate towards the main duct exit is greatly reduced, the pressure drop between the interface region and the exit is also reduced, resulting in higher pressure here also. Although there is some scatter in the data,

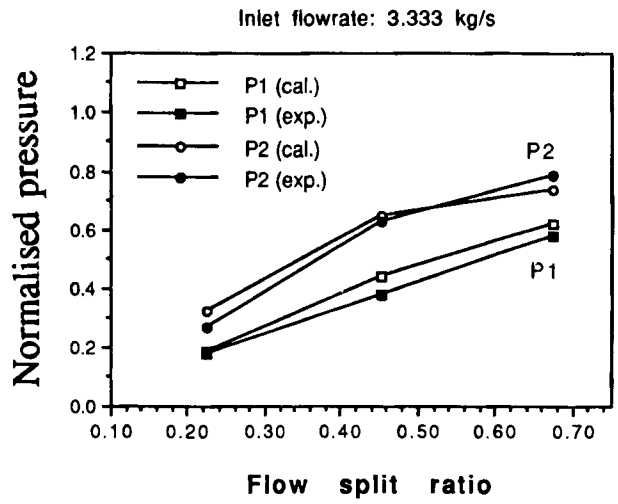

Figure 10. Effect of flow split ratio on normalized pressure

as mentioned above, the increase in the exit pressure (P_2) with flow split ratio is greater than that in the inlet pressure level (P_1).

An increase in flow split ratio has virtually the same effect on the flow rates Q_1 and Q_2 through the two branches, as shown in Figure 11. For the flow split ratios shown, the variations are essentially linear and the lines are parallel. As the flow split ratio tends to zero of course, both these lines must also tend to zero, hence no longer being parallel. For all flow split ratios examined, the flow through the second branch is higher than that through the first. There is no evidence to suggest any difference would be found as the flow split ratio tends to its asymptotic

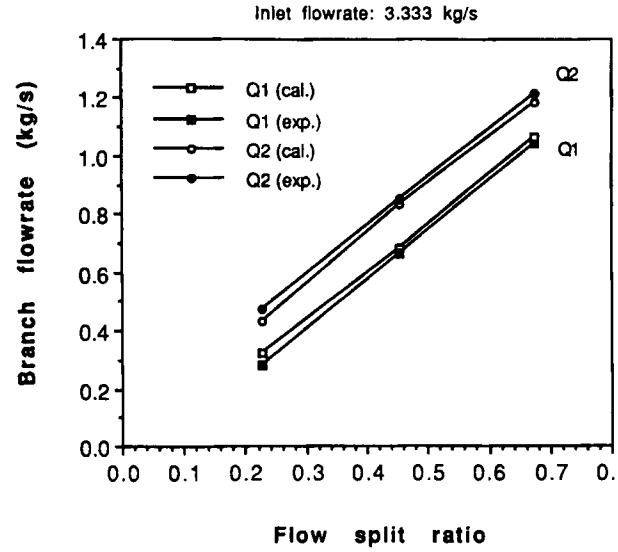

Figure 11. Effect of flow split ratio on branch flow rate

value of unity. The fact that these two lines are parallel means that the difference in flow rate between the two branches is independent of flow split ratio. Thus the unevenness of flow rate distribution is relatively more significant at low flow split ratios. The agreement between calculations and experiment shown here is reasonable, with an underprediction of the unevenness of flow rate distribution between the branches. For the lowest flow split ratio examined, the difference between the flow rates in the two branches is underpredicted by 40%, whereas at the highest flow split ratio it is underpredicted by less than 20%.

The size and shape of the recirculation regions in the branches vary significantly with flow split ratio. The shape of the recirculation region is represented by the separation streamline in the plane of symmetry, although the shape will vary across the duct. The streamline curvature is a result of the velocity and pressure gradients normal to the streamlines, which are strongly influenced by the flow rate through the branch. The values of the lengths (L_1 and L_2 for branches 1 and 2 respectively) and widths (W_1 and W_2 for branches 1 and 2 respectively) of the recirculation region in the plane of symmetry give useful indications of the flow blockages presented by the recirculation regions. Figure 12 shows that the length and width both decrease with flow split ratio and that the length is affected more strongly than the width (but not necessarily in percentage terms). In other words, the more flow there is into the branch, the smaller is the blockage caused by recirculation. Measurement and prediction also show that the width and length of recirculation for the second branch are smaller than those for the first. This trend holds for all the flow split ratios examined.

Effect of inlet flow rate

The flow rate at the inlet of the main duct has a complex effect on the structure of the flow. For example, the size and shape of the recirculation region in a single branch are significantly

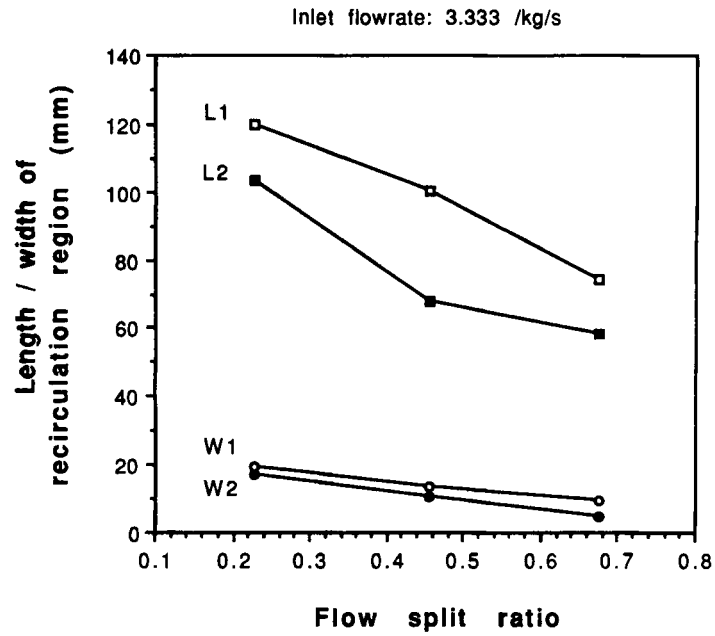

Figure 12. Effect of flow split ratio on recirculation region size

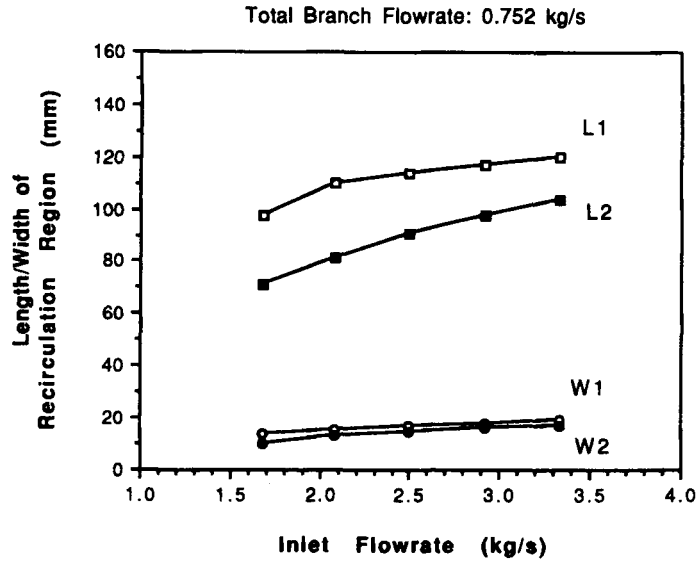

Figure 13. Effect of inlet flow rate on recirculation region size

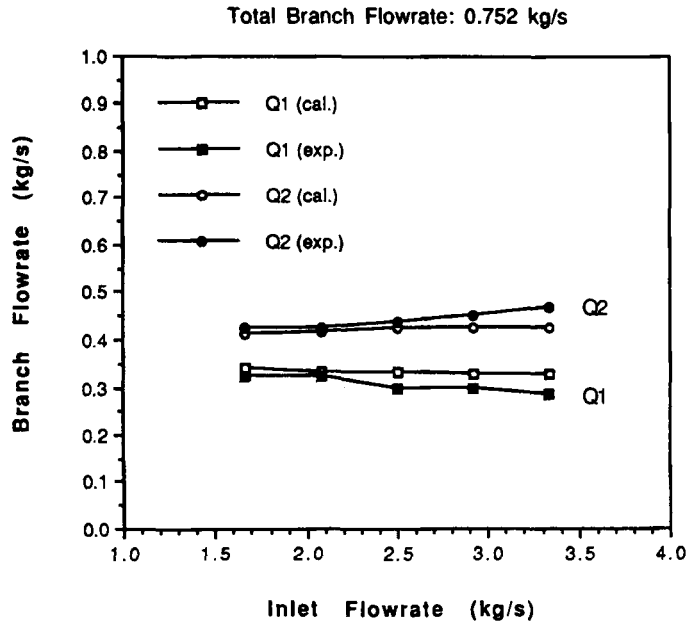

Figure 14. Effect of inlet flow rate on branch flow rate

affected by the inlet flow rate when the flow split ratio is kept constant, as observed by Fu *et al.*[8] Further investigation of the effects of the inlet flow rate was carried out for the two-branch flow. Computations were performed for five inlet flow rates, namely 3·33, 2·92, 2·50, 2·08 and 1·68 kg s^{-1}, and characteristic results are presented in Figures 13 and 14. The sizes of the recirculation regions increase with inlet flow rate when the total flow rate through the branches is held constant, although the effect is much greater on the length than on the width. These

effects occur presumably because of the increased velocity component W at the inlet to the branches for an increased total flow rate and the variation in pressure which this causes. The effects are greater on the second branch because of the flow distribution between the branches, as illustrated in Figure 14. The flow rate in the first branch tends to decrease and that in the second branch to increase with an increase in total flow rate. This trend was observed experimentally to be more significant than was predicted. These variations must be due to variations in the pressure levels in the main duct/branch interfaces.

The present study of the effects of flow split ratio and inlet flow rate has shown that the flow structure is a complex function of many variables. The recirculation region is affected by both flow split ratio and inlet flow rate, for example, and it can be expected to be also affected by geometric factors such as the angle of the branch with the main duct, the cross-sectional shape of the branch, etc. These effects are certainly worth investigating.

The above results show that the parallel experimental and theoretical approach is suitable for the study of inlet manifold flows. Further measurements and calculations are in progress to identify the influence of the geometry of the manifold on the flows.

4. CONCLUSIONS

1. A finite volume computational fluid dynamics code employing the k–ε model for turbulence has been developed to predict three-dimensional turbulent dividing flows in multibranch manifolds. The numerical prediction was extensively validated against experimental data and reasonable agreement between prediction and measurement has been obtained. It is shown that the developed numerical code is capable of capturing all major features of the flow.
2. The flow structure was strongly three-dimensional and remained similar for all the cases examined. Secondary motion downstream of the junction interfaces both in the main duct and in the branches is one of the common features of the flow; these motions become more pronounced at higher split ratio. Therefore the secondary flow and its associated pressure loss may not be neglected at high flow split ratios.
3. Flow separation takes place in each of the branches and a recirculation region is formed. The size and shape of the recirculation in a branch varies with flow split ratio and inlet flow rate. The velocities downstream of the junction in the main duct are significantly affected by the flow split ratio.
4. The turbulence energy is generally higher in the branch than in the main duct and increases with flow split ratio.
5. A large pressure gradient was observed in the junction region and it is responsible for the change in flow direction. The lowest pressure was found in the recirculation region.
6. The flow pattern remains similar in different branches of a manifold, but there are significant differences in flow rate, recirculation region size, turbulence energy, etc. The flow rate is always greater and the recirculation region is always smaller in the second branch than in the first branch. The turbulence energy levels are generally higher in the second branch.

ACKNOWLEDGEMENT

The authors are pleased to acknowledge financial support from the Science and Engineering Research Council under grant GR/H16346 for the work presented in this paper.

APPENDIX: NOMENCLATURE

d	branch hydraulic diameter
D	main duct hydraulic diameter
FSR	flow split ratio (total branch flow rate/main duct inlet flow rate)
k, ε	turbulence kinetic energy and its dissipation rate respectively
L_1, L_2	lengths of recirculation regions in branches 1 and 2 respectively
P	pressure
P_1, P_2	normalized pressures at inlet and exit of main duct respectively
Q_1, Q_2	mass flow rates in branches 1 and 2 respectively
U, V, W	velocity components in x-, y- and z-directions respectively
v^1	RMS velocity in y-direction
W_1, W_2	widths of recirculation regions in branches 1 and 2 respectively
x, y, z	Cartesian co-ordinates

REFERENCES

1. R. Margary and E. Nino, 'The effect of intake duct length on the in-cylinder air motion in a motored diesel engine', *SAE Paper 900057*, 1990.
2. C. Arcoumanis, P. Flamang and J. H. Whitelaw, 'Flow in the inlet manifold of a production diesel engine,' *Proc. Inst. Mech. Eng.*, **203**, 39–49 (1989).
3. R. S. Benson, *The Thermodynamics and Gas Dynamics of Internal Combustion Engines*, Vol. 1, Clarendon, Oxford, 1982.
4. M. Chapman, J. M. Novak and R. A. Stein, 'Numerical modelling of inlet and exhaust flows in multi-cylinder internal combustion engines,' *Flows in Internal Combustion Engines, ASME Winter Ann. Meet.*, Phoenix, AZ, 1982, ASME, New York, 1982.
5. A. Pollard and D. B. Spalding, 'The prediction of the 3-D flow field in a flow-splitting tee junction', *Comput. Methods Appl. Mech. Eng.*, **13**, 293–296 (1978).
6. M. Chapman, 'Two-dimensional numerical simulation of inlet manifold flow in a four cylinder internal combustion engine', *SAE Paper 790244*, 1979.
7. M. A. Leschziner and K. P. Dimitriadis, 'Numerical simulation of three-dimensional turbulent flow in exhaust manifold junctions', *Proc. Inst. Mech. Eng. Conf. on Computers in Engine Technology*, Cambridge, 1987, Institution of Mechanical Engineers, London, 1987.
8. H. Fu, A. P. Watkins, M. J. Tindal and M. Yianneskis, 'Computation of three-dimensional turbulent flows in a pipe junction with reference to engine inlet manifolds,' *Proc. Inst. Mech. Eng., J. Mech. Eng. Sci.*, **206**, 285–296 (1992).
9. H. Fu, A. P. Watkins and M. Yianneskis, 'Three dimensional simulation of turbulent flow in a four-branch manifold', *Proc. Inst. Mech. Eng. Conf. on Engineering Applications of Computational Fluid Dynamics*, London, 1993, Institution of Mechanical Engineers, London, 1993.
10. M. A. Leschziner and K. P. Dimitriadis, 'Computation of three-dimensional turbulent flow in non-orthogonal junctions by a branch-coupling method,' *Comput. Fluids*, **17**, 371–396 (1989).
11. B. E. Launder and D. B. Spalding, Computer Methods in Applied Mechanics and Engineering, Vol. 3, *The Numerical Computation of Turbulent Flows*, North-Holland, Amsterdam, 1974.
12. B. E. Launder, 'Second moment closure and its use in modelling turbulent industrial flows', *Int. j. numer. methods fluids*, **9**, 963–985 (1989).
13. K. V. Patankar, *Numerical Heat Transfer and Fluid Flow*, Hemisphere, New York, 1980.
14. K. P. Dimitriadis and M. A. Leschziner, 'Computation of three-dimensional duct junction flow by a zonal approach,' *Proc. 4th Int. Conf. on Numerical Methods in Laminar and Turbulent Flow*, Swansea, 1985.
15. H. Fu, A. P. Watkins, M. J. Tindal and M. Yianneskis, 'Turbulent dividing flow in a branched duct,' *Proc. Fourth Int. Conf. on Laser Anemometry—Advances and Applications*, Cleveland, OH, 1991.
16. T. Kobayashi, H. K. Myong and M. A. Ohmachi, 'Numerical investigation of modified k–ε turbulence models for the simulation of a backward facing step flow', *Eur. Engineering Research and Technology Transfer Congr.* 1991, Paper C413/014.
17. P. G. Huang and M. A. Leschziner, 'Stabilization of recirculation-flow computations performed with second-moment closures and third-order discretization,' *Proc. Fifth Symposium on Turbulence Shear Flows*, Cornell, NY, 1985.
18. A. M. K. P. Taylor, 'Confined isothermal and combusting flows behind axisymmetric baffles', *Ph.D. Thesis*, University of London, 1981.
19. B. P. Leonard, 'A stable and accurate convective modelling procedure based on quadratic upstream interpolation', *Comput. Methods Appl. Mech. Eng.*, **19**, 59–98 (1979).